ISSN 2320-9186

Topic:

Satellite and Radar Remote Sensing approach for forecasting and analyzing the effect of the tropical cyclones Pam over the southwest Pacific.

Abstract

Tropical cyclones are feared natural disasters that frequently have devastating effects over the southwest pacific. Since their impact classification varies greatly in the social and human contexts, the present study focuses on analyzing the structure and intensity of TC as well as precipitation patterns using satellite remote sensing. Then, in order to support the observation and forecast of the TC using remote sensing, this study focus on improving the key features for interpreting satellite and radar image to support observation and forecasting of TC in the southwest pacific. Thus, provide a wealth of evidence supporting the significance and value of remote sensing, including the ability to the track formation and evolution of the TC Pam; estimate the maximum intensity and turbulence intensity; provide a helpful guide for civil protection measures and activities and assess the degree of damage to many components, including ecosystems and anthropogenic structures.

Keyword

Vanuatu, Forecasting, Tropical cyclones (TC), Remote Sensing, and satellite.

Introduction

One of the most dangerous atmospheric circulations is the tropical cyclone (TC), which is an expensive disaster and has the capacity to seriously harm people, society, transportation, and property over the southwest pacific.

A TC is a region of high winds and low pressure. Severe storms must combine with the atmosphere and ocean to develop into TC. The ocean water first requires its temperature to be warmer than 26.5 °C to a depth of 50m and weak vertical wind shears are the conditions that typically cause TC to form over tropical oceans [1, 2] and if the atmosphere is favorable, it can intensify quickly. TC is fueled by the moisture and heat of warm water and can quickly dissipate on land or in colder ocean areas where heat and moisture sources are not limited, besides the low and middle troposphere relative humidity is necessary for TC development.

Furthermore, the low central pressure and inwardly rotating winds characterize TC, in the Southern Hemisphere wind rotate counterclockwise due to the Coriolis effect, and the diameter of the TC can range from 100 to 2000 km, with an average of 200 to 500 km and 1500 feet height at which TC winds are strongest and that drops above and below with potential to seriously harm on the surface.

Moreover, the crucial characteristic of TC is its vertical wind shear which helps the TC to develop vertically as the wind shear is weak, and the latent heat from condensation aids in this process also TC are tilted and their latent heat release is stretched out by stronger wind shear.

Therefore, TC receives its energy from the ocean, making them resemble heat engines, and convective cloud towers are produced by the evaporation of warm ocean water and are fueled by latent heat that is released as the air cools and condenses as it rises.

In fact, the potential for devastating destruction to human lives, civilization, transportation, property, etc. makes TC one of the most dangerous weather systems. For instance, TC Pam, which hit Vanuatu on 13 march, 2015, with a maximum wind speed of 280 km/h, affected the whole island of Vanuatu. It was the most expensive TC in Vanuatu's history, killing 11 people and 166,600 people were affected causing $443 million in damages [3, 4].

Remote sensing satellite and radar remote sensing is the ultimate way to identify and keep track of TC activities in the southwest pacific since TCs spend the majority of their lives far from land.

This study will be focusing on multi-Satellite and Radar Remote Sensing ability and error correlation with an approach for forecasting and analyzing the effect of TC Pam, to determine TC Pam intensity, formation, movement, precipitation, damage, and surrounding weather phenomena.

Section 1 discusses general information about TC including TC observation, season, classification, life cycle, and favorable environmental conditions for TC formation while **section 2** discusses the remote sensing approach of TC structure analyses and intensity estimation. **Section 3** is about TC forecasting with a remote sensing aspect. **Section 4** is on TC Pam analysis including intensity estimation and eyewall replacement cycle with support to climate

effect on the impact of TC Pam and **section 5** is Discussion and Conclusion.

1 TC Observation

The TC season in Vanuatu runs from November to April. Due to its location in the southwest Pacific, TC has winds of at least 34 knots (62 km/h) and may pass through Vanuatu. Vanuatu (land and sea) experiences 2-3 cyclones per season, most often in January and February. Vanuatu's marginal seas see 20 to 30 cyclones per decade, with 3 to 5 causing catastrophic damage [5].

Pacific's extensive coastline, which has a high population density, is vulnerable to these natural hazards, making it one of the most cyclone-affected places in the world in terms of fatalities. The severity of the storm surge produced by TC varies from place to place for the same TC intensity due to the varied coastal bathymetry of the coast of the pacific island. For the exchange of messages among the panel countries, the classifications of TC disturbances over the pacific region are provided below. Classification: A tropical depression has sustained winds of 38 mph or less. Tropical Storm: TC with 39-73 mph winds (34 to 63 knots). A TC Category 5 has sustained winds of 74 mph or more [6].

TC frequently have a long lifespan, up to two or three weeks over tropical ocean waters, they may begin as a group of thunderstorms [7]. After a disturbance has developed into a tropical depression, it can take a few days or a half-day to progress to the next stage as a tropical storm. The same could apply to how long it takes a tropical storm to develop into a TC. The main factors influencing these

phenomena are oceanic and atmospheric variables. A continuous process for TC is represented by the four stages listed below. Depending on the storm's life cycle, some stages may even repeat themselves.

Their surface winds oscillate in cycles (clockwise in the Southern Hemisphere). A TC eyewall, which encircles a fairly calm eye at the warm center of the storm, is where the storm's strongest winds are found. The eye of a hurricane often has a diameter of tens of kilometers. Very heavy rain can be produced by clouds in the eyewall as well as the spiral bands outside the eyewall.

Condition for TC formation, according to statistical analyses of the observed climatology of TC.

1. A sea surface temperature of at least 26.5°C down to a depth of 50 m, so that breezes cannot easily mix deep cooler water with the surface (situation of deep thermocline).

2. Sufficient north or south of the equator, as previously predicted, for the Coriolis force to be considerable and aid in the convergence of the air masses at the surface (usually at least 4-5℃ in latitude).

3. A previous disturbance that has cyclonic circulation (i.e., a significant low-level vortex) and has persisted for more than 24 hours. Since the angular momentum of the disturbance's air is preserved as it converges, a rise in wind speed is expected.

4. Low levels of vertical wind shear, or the change in wind speed with height, from the Earth's surface to the upper troposphere (about

13 km or 8 miles up). According to [8], such a scenario may favor the introduction of dry air into the storm system.

5. Sufficient water vapor in the middle troposphere. Dry air can occasionally be found in the center of the troposphere over tropical oceans; this dry air suppresses thunderstorms and prevents the formation of tropical depressions. On the other hand, if the humidity level in the troposphere is too high, the disturbance won't be able to moisten the air enough for tropical storm genesis to take place (through evaporation from the ocean surface).

6. "An atmospheric vertical temperature profile that cools with height sufficiently to enable TC activity."

The so-called storm surge, or water piling up above the regular sea level, is one of the significant effects of the TC's powerful wind circulation. It has been established that the highest sustained wind or sea level pressure at the TC center directly correlates with the sea level surge brought on by a TC that makes landfall. In those areas affected by the TC landfall and subsequent storm surge effect, the combined impacts of low pressures, powerful waves, and local sea level rise can substantially take advantage of unfavorable bathymetry to generate extensive flooding (Figure 1).

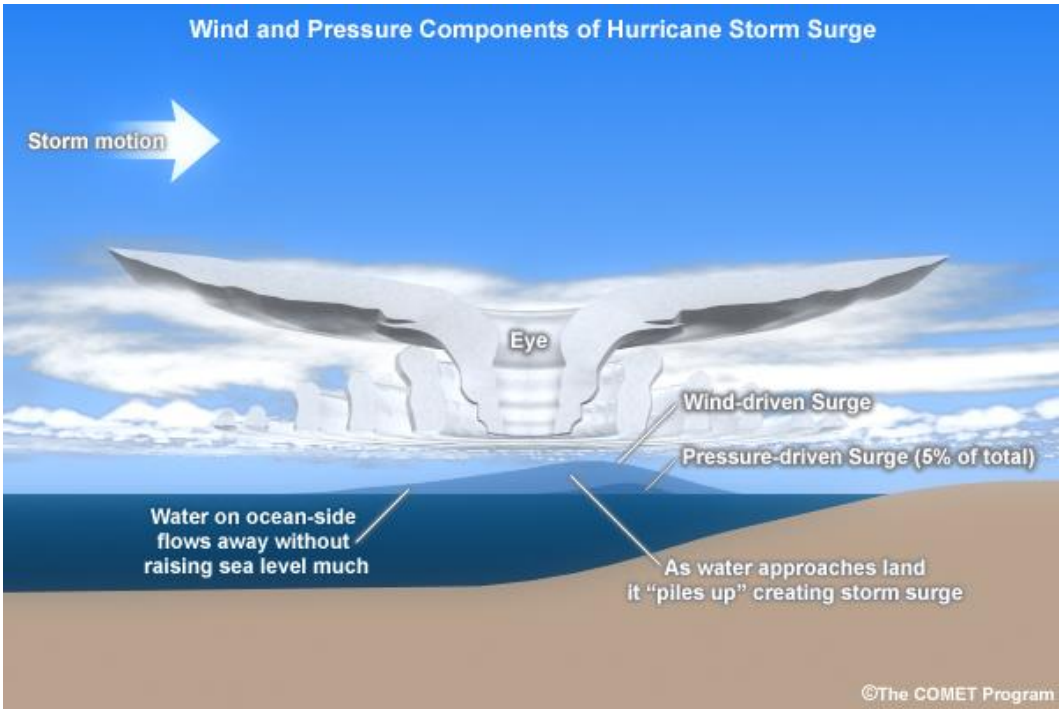

Figure 1. Storm surge effect. Courtesy of the UCAR Comet Program.

7. Because they feature warm (not cold) core central lows and wind speed decreases with height, TC has a different vertical structure than storms at mid-latitudes. Additionally, while jet streams are typical of mid-latitude perturbations, they are not present aloft above TC.

2. Remote sensing approach

Systematic TC intensity analyses from imagery started not long after the first satellite weather measurements were made available [9]. Up until the significant work of Dvorak [10] in 1972, the only consistently produced operational use of TC satellite analysis was to determine the TC center position. Dvorak created an empirical model based on visible channel cloud organization to identify TC intensity. Structural characteristics like brightness, warmth, banding curvature, and cloud pattern distortion were factors that contributed to the storm's severity. To reliably derive subjective estimates of TC intensity from the structural clues in satellite data, a flowchart of Dvorak technique rules was developed. Dvorak improved his technique over time by adding more guidelines and restrictions as well as the usage of infrared channels to increase accuracy and lessen subjectivity.

The Operational analysis uses Dvorak. It remains the most common TC intensity diagnosis method. Update the intensity-defining wind-pressure relationship [11]. Dvorak analysis' global applicability and customizable [9] make it a versatile TC forecasting tool. The Advanced Dvorak Technique (ADT) [12] made TC intensity analysis more objective by automating it [13].

Dvorak and other infrared and visible methods can assess TC structure and intensity. RMW, 34, 50, and 64 kt winds were associated with infrared TBs in 2007 [14]. Similar infrared imaging resolved TC sizes, determined by the radius of the 5 kt 850 hPa wind, that relate to TC lifetime [15]. The deviation angle variance

technique analyzes temperature distributions for TC axisymmetric to detect structure, centering, origination, and intensity [16].

GEO water vapor and infrared channels may relate TC intensity and structure changes [17]. The weighting function representing variable heights and chemical profiles highlights structural elements like overshooting convective tops. Finally, IR rotational speed and visible cloud tops near the TC core are associated with major northwestern Pacific basin typhoons [18].

TCs can be observed using remote sensing frequencies other than infrared and visible channels. Through the use of surface wind data, satellite active microwave radars (scatterometers) have aided the National Hurricane Center (NHC) in determining the size and severity of storms [19]. The surface wind vector can be calculated using scatterometers pulses that bounce off the ocean's surface due to wind roughening. The storm size climatology at 23 kt and an outer radius was produced using QuikSCAT scatterometers data and a wind structure model [20]. A QuikSCAT climatology of storm sizes was developed for the 34-kt radius and outer-core strength (OCS) intensity [21–23] through similar investigations. When determining the frequency thresholds across TC zones, the TRMM precipitation radar (PR) and TMI are employed [24]. SAR subjectively categorized ocular qualities as spatial extent, shape, and wavenumber while visualizing incredibly minute mesoscale elements of TC [25]. Unlike visible and infrared channels, passive microwaves can directly analyze TC structure by penetrating cloud tops that aren't raining [26]. Radar retrievals from space are uncommon, and SAR TC retrievals have poor physical connections.

The two main categories of polar-orbiting microwave sensors are imagers and sounders. The sensors used in microwave imagers typically evaluate surface characteristics as well as the arrangement of different water phases in the atmosphere. The goal of the microwave sounders is to offer profiles of the moisture and satellite remote sensing of TC assessments of the atmospheric thermal structure. There may be channel overlap between a microwave imager and a sounder depending on the objectives of a given sensor.

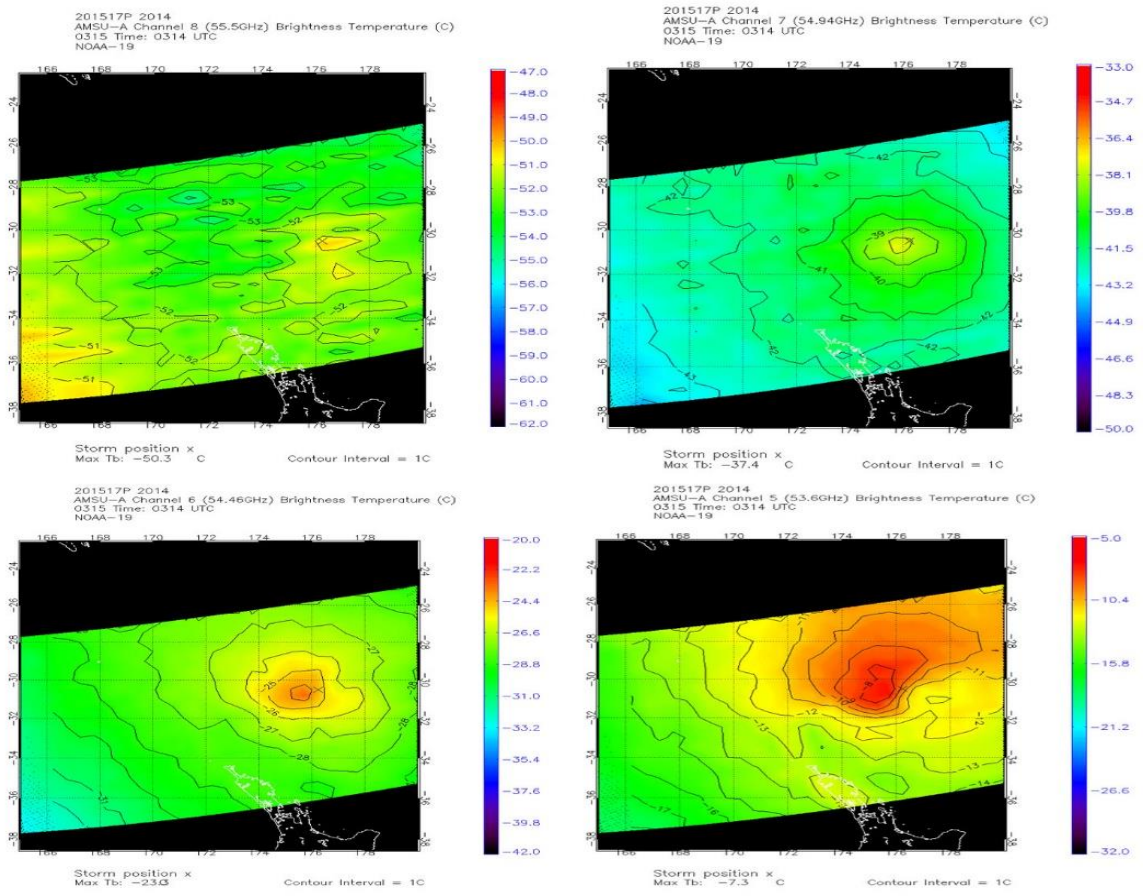

Figure 2. AMSU Temperature for TC Pam on March 15, 2015.

Soon after their launch, microwave sounders were utilized to assess TC structure and intensity [27]. Advanced sensors, such as AMSU, are beginning to resolve thermal anomalies and core/eye size [28,

29]. Storm features have generally been rounded off by sounders, making analysis challenging. Figure 2 displays the distributions of temperature anomalies during TC pam, which occurred from March 09 to March 16, 2015. It shows how the amplitude of the distinctive TC upper-level warm core signature increases as the intensity of the storm increases. Maximum sustained wind (MSW), minimum sea level pressure (MSLP), and wind radii at 34, 50, and 64 kt can all be calculated using multiple linear regressions of AMSU channels [30]. Of all satellite-based intensity estimating techniques, the satellite consensus (SATCON) method has the highest skill [31]. It uses the ADT and two AMSU intensity estimations. Retrieving TC structure might be enhanced by using AMSU data as part of an ensemble.

Despite its recent introduction, there have been some advancements in the study of TC employing microwave imagers. For instance, the NHC makes considerable use of microwave imagery to more accurately locate a TC core and determine subjective structural changes [32]. To enable a visually appealing representation of TC structure changes, the Morphed Integrated Microwave Imagery at CIMSS (MIMIC), a method to construct “morphed” animations of passive microwave imagery employing an advection function between satellite passes, was developed [33]. The relationship between microwave imager data and TC intensity was also demonstrated by other investigations [34, 35]. Early detection of a developing eyewall using the microwave data has improved TC intensity estimations [36], and a color composite of the H, V, and PCT data at 37 GHz created at NRL-MRY has shown great promise in identifying the creation of a TC inner core [27]. To forecast the

quick intensification of TC at the outset, a symmetrical and closed TB threshold (the “cyan ring”) was used [37].

Many of the physical mechanisms underlying TC intensification and decay are challenging to study and have little understanding.

Therefore, cyclone strength prediction is a more challenging task than track prediction. Among the variables that affect TC intensity are (Figure 3)

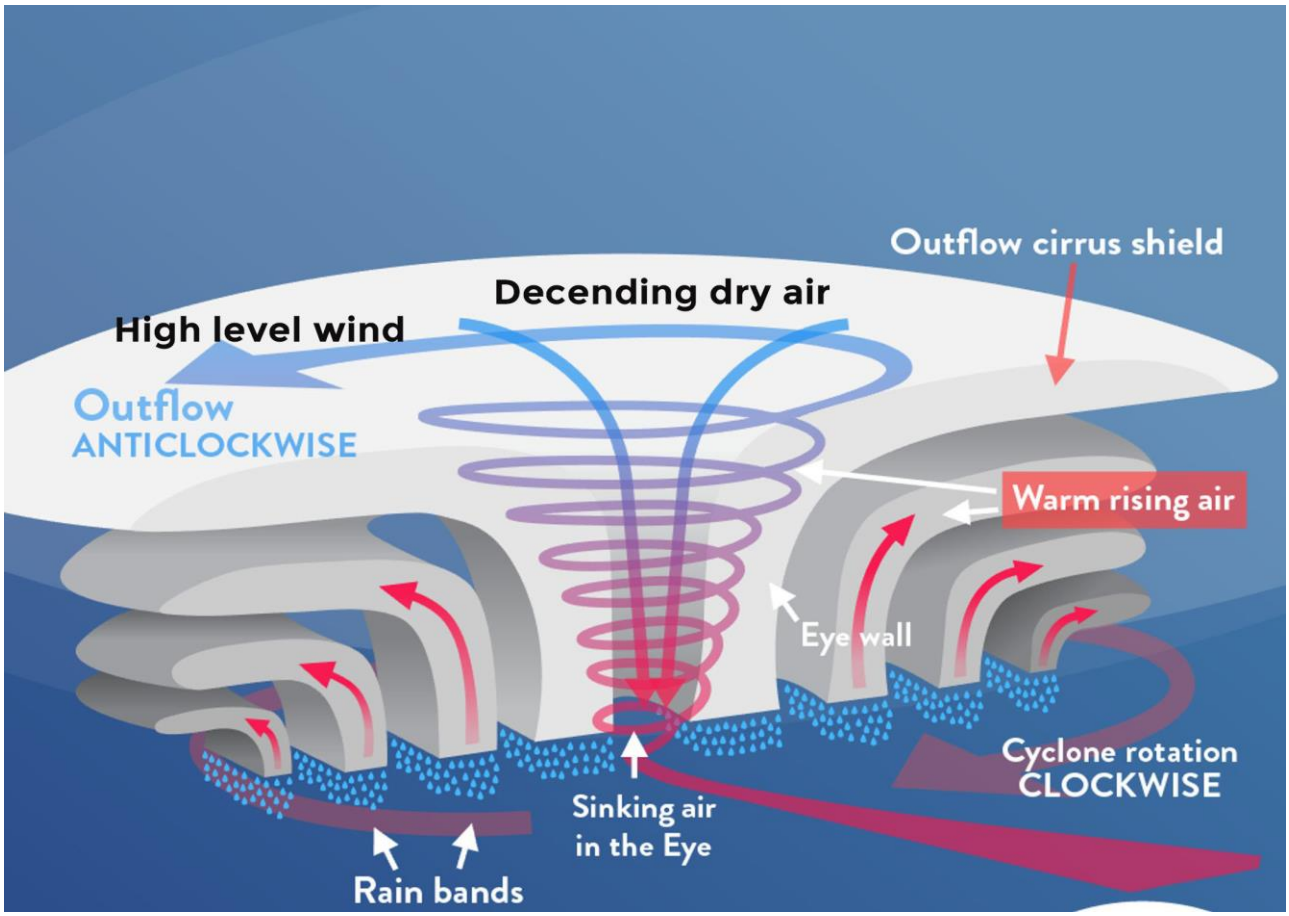

Figure3. The intensity structure of TC over the southwest pacific

3. TC Forecasting over the Southwest Pacific

Before landfall, satellite-based microwave scatterometers measure the speed and direction of the near-surface wind. Although eyewalls are frequently seen to be roughly circular, they can also take on polygonal shapes on occasion. The basis on the theoretical dynamics, numerical simulations, and observations in liquid water, it was theorized that the polygonal structures were related to mesovortices. Recent observational research confirms the existence of mesovortices within the eye by demonstrating pentagon-shaped reflectance patterns (Fig. 4c, d). Because they are part of the eyewall convection and have a considerably smaller horizontal scale than the eye, these eyewall mesovortices are deep vortex structures. Vortices in the eyewall may experience 10% higher wind speeds than the remainder of the eyewall. The polygonal shape of the cloud pattern is produced by adding the flows connected to the mesovortices to the flow in the eye.

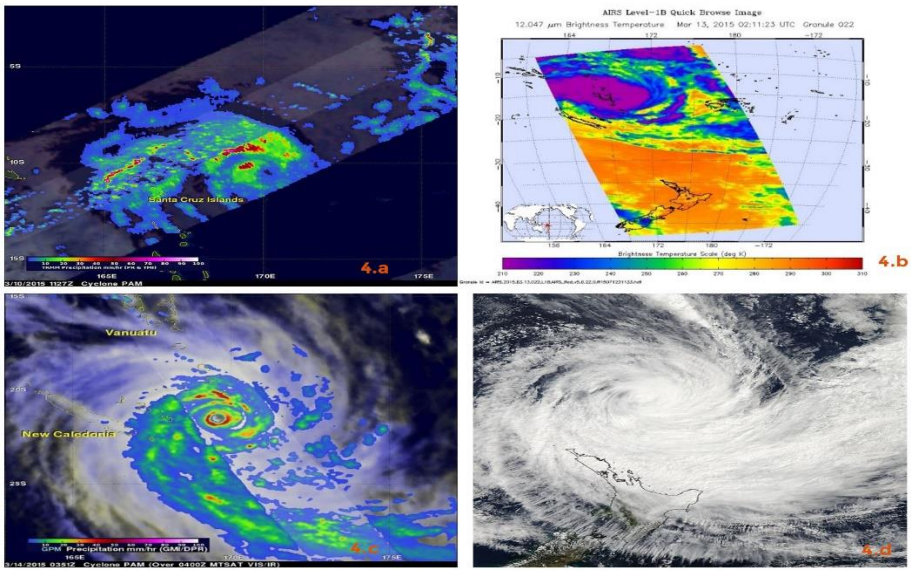

Figure 4. satellite and airborne radar image of tropical cyclone pam. (a) TRMM image on march 10 2015; (b) 12.047mu Bright

Temperature at 021123 UTC on 13 march 2015; (c) NASA-JAXA's GPM core satellite image at 0351 UTC on march 14 2015; and (d) MODIS instrument aboard NASA's Aqua satellite image at 0205 UTC on march 15 2015.

In order to comprehend how changes in a TC inner core affected were affected by changes in intensity, the 2015 Cyclone Rain Band and Intensity Change Experiment (RAINEX) made precise observations in the inner cores of TC Pam 2015, TC Winston 2016, and TC Harold 2020. A variety of intriguing characteristics that have never before been seen are depicted in Fig. 5, including rain bands with very high reflectivity that are oblique to the concentric eyewall. As they migrate across the eyewall, these formations are influenced by various winds and offer hints about how eyewalls evolve during sudden variations in intensity. They seem to resemble the structures that theoretical studies and numerical models have anticipated.

MTSAT-2 10.8 μm IR Reflectivity Composition Image of TC Pam 0032 UTC 13 march 2015

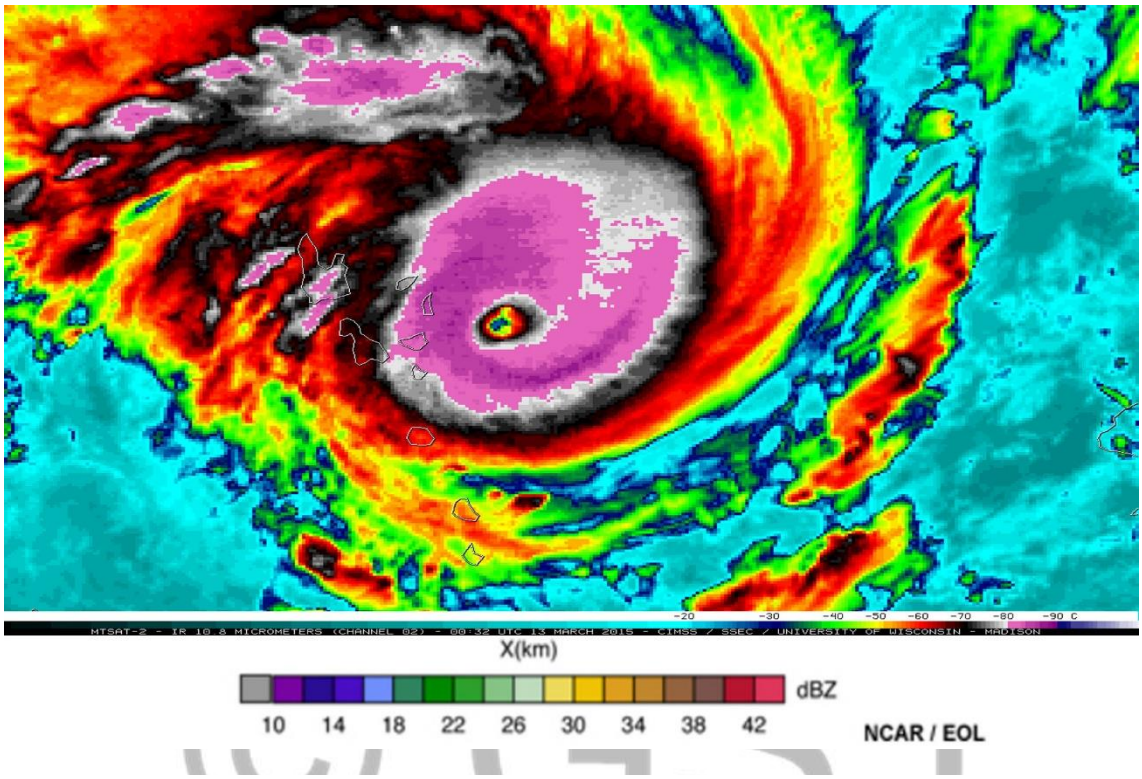

Figure 5. Radar reflectivity composition image of TC Pam taken by MTSAT-2 10.8 μm IR, 13 march 2015, during the TC rain band and intensity.

The hydrometeors (droplets or ice crystals) inside the eyewall and rain-bands severely attenuate microwave wavelengths, microwave radiometers can detect the interior TC structure, such as the location of the eye. While this is going on, IR techniques only see the cloud tops, and dense cirrus can obscure the underlying TC structure.

For instance, it is challenging to distinguish the eye of TC Pam from the IR photos in Fig. 6 (below) (upper panels). However, the eye is noticeable (bottom panels) in the 85 GHz microwave photos, giving a trustworthy signal of a strengthening TC. Additionally, the area of the

cool cloud to the right of the eye in the IR image does not correspond to deep convection; it appears blue in the microwave image.

Sadly, microwave equipment is carried by low-earth orbiting (LEO) satellites that can only examine a given storm twice every day. As the network of LEO satellites keeps growing, it has become more typical to get many daily images of the same TC. Microwave scans, which reveal the inside structure of TC, are useful for locating powerful TC, many of which include concentric eyewall structures.

Multisensory image of TC Pam, 13 march 2015

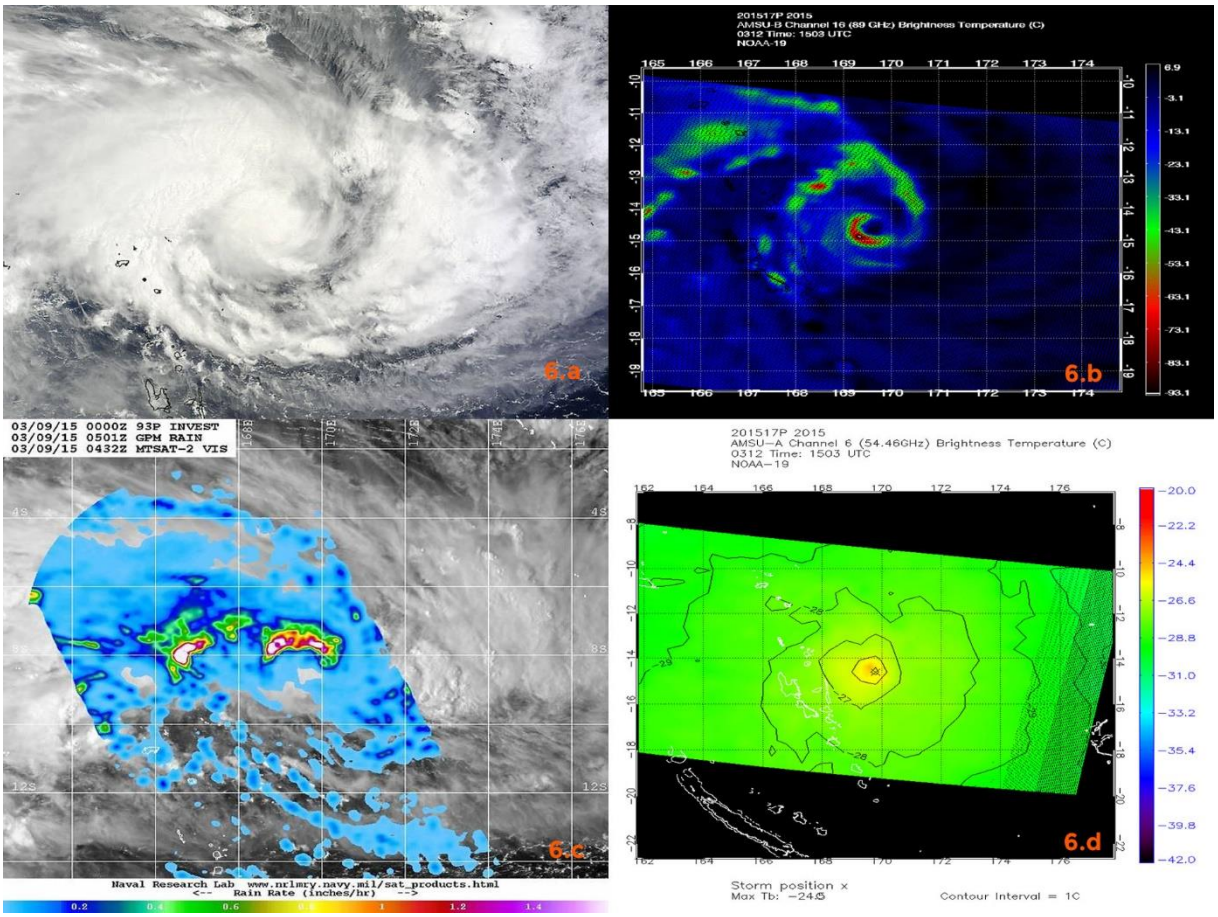

Figure 6. TC Pam 2015 observation by geostationary grayscale IR and enhanced IR-BD and polar orbit microwave 85 GHz sensor.

It is crucial to take into account TC strength in terms of various wind speed radii that are crucial to decision-makers, in addition to the central pressure or the radius of maximum winds. Based on parameters like the radius of gale-force winds, the width of evacuation zones is determined (1-minute sustained surface winds between 17 and 24 m s-1). Estimates of wind speed are essential for forecasting storm surges. TC Pam in 2015 had a gale force wind radius of only 55.5 km.

Satellite-based microwave scatterometers monitor the backscatter from small-scale waves on the ocean surface and connect the backscatter to wind velocity, allowing for the observation of near-surface wind speed and direction prior to impact. Outside of the high-wind and high-precipitation region of the eyewall, moderate-wind and low-precipitation situations are where microwave scatterometers often work at their best. Cloud drift winds also offer estimates of winds outside of heavy convection; however, they are constrained by errors in height assignments. Examples of satellite-derived winds in and around TC Pam are shown in Figure 7.

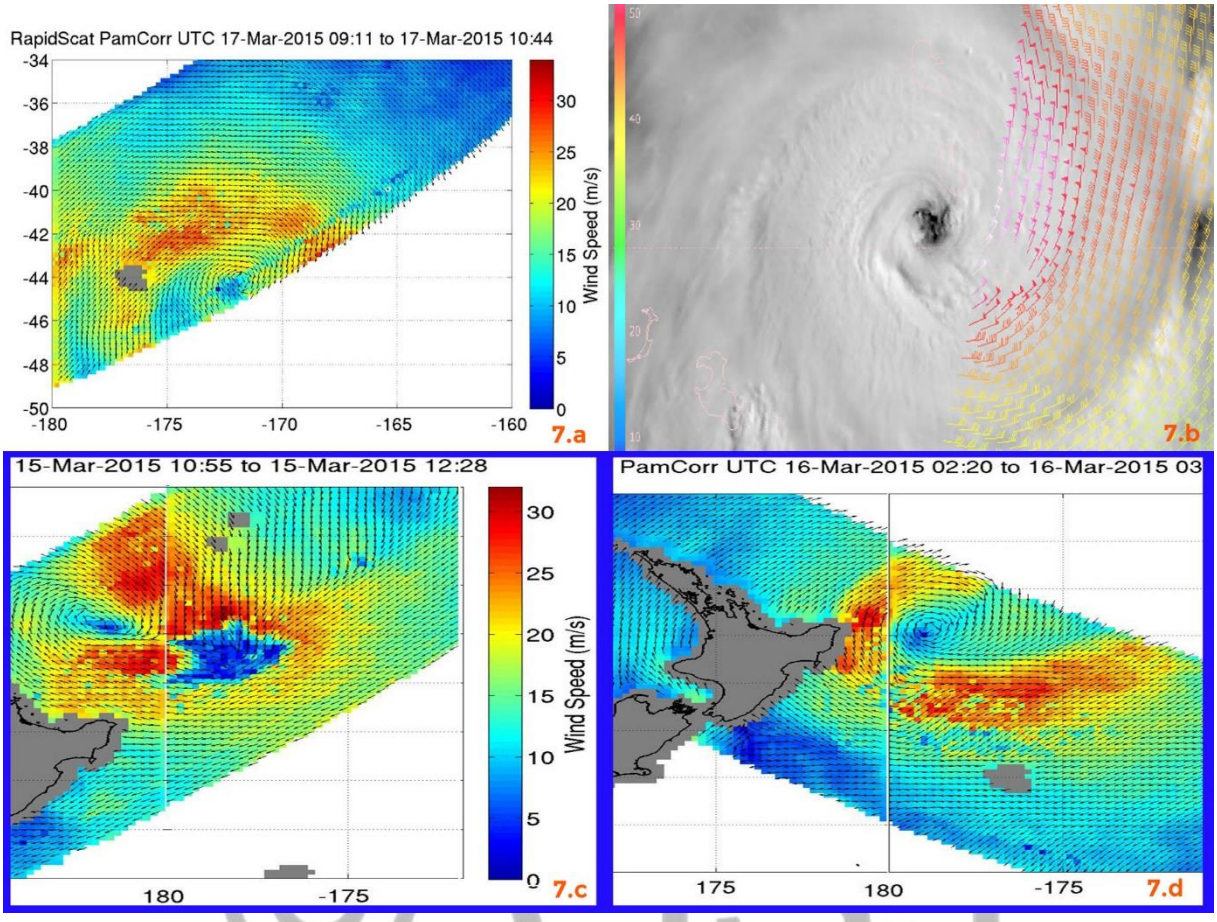

Figure 7. Satellite-derived winds of TC Pam; (a,c,d) are radar images of TC Pam from 15-17 March 2015; (b) satellite images of TC Pam on 13 March 2015.

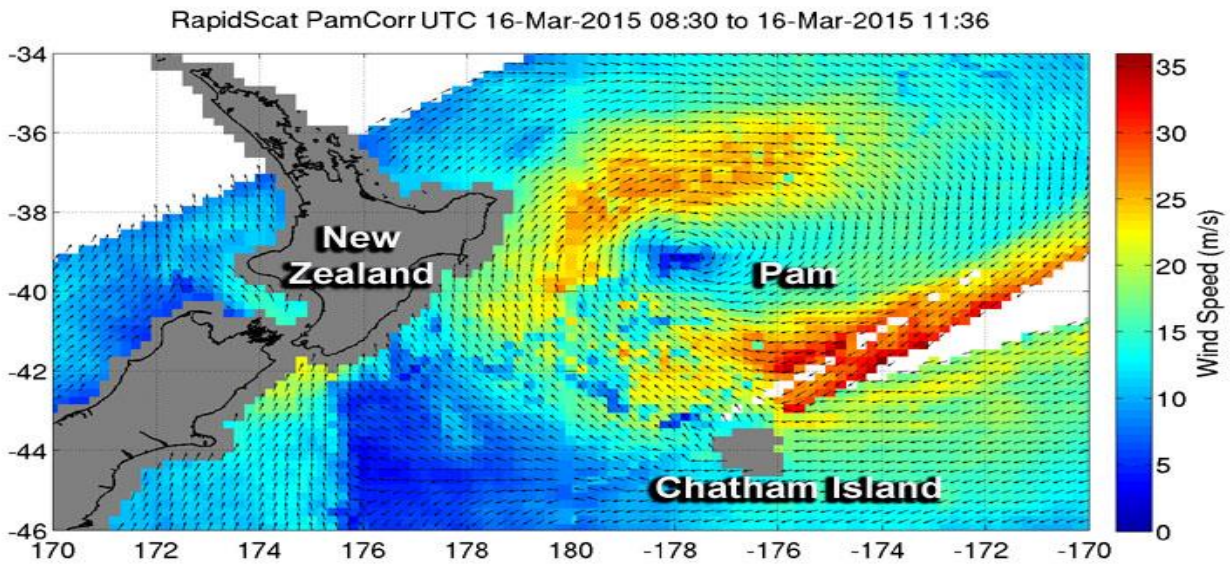

Figure 8. RapidScat revealed sustained winds over 30 meters per second/108 kph/67 mph (in red) were still occurring southeast of Pam's center on March 16.

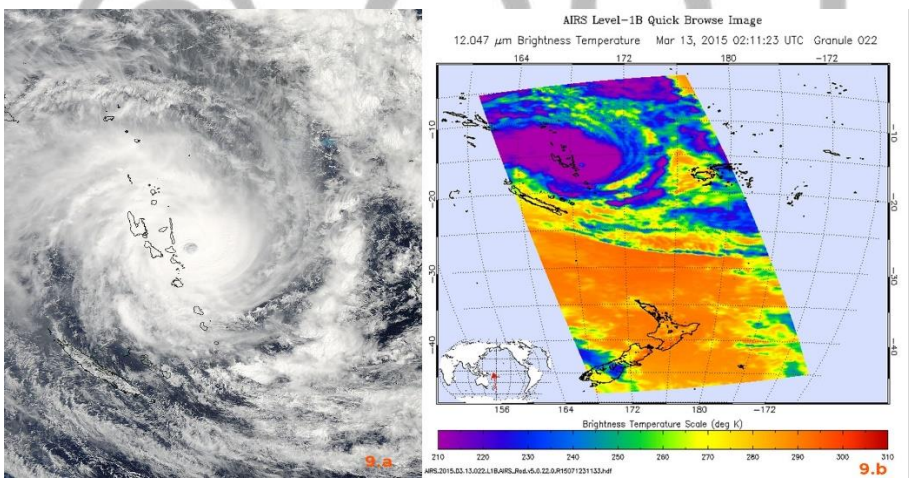

Figure 9. (a)satellite image of TC Pam on March 13, 2015; (b)12.047µm brightness temperature on March 13, 2015.

4. TC Pam analysis

With the exception of the Northeast Pacific, where aircraft reconnaissance flights are frequent, the conventional method of determining TC intensity involves analyzing geostationary longwave (IR) imagery. The intensity can be adjusted for continuous operational forecasting with frequently accessible geostationary IR pictures (15–30 minutes typically and 5 minutes in rapid-scan mode).

A classification system for determining the strength of TC from satellite data was established by Vern Dvorak in 1975.

The "Dvorak Technique," which was created with the aid of empirical data, connects a numerical index (known as the current intensity or CI) to a prediction of the maximum sustained winds (MSW) at the surface (Table 1)

Intense convection and changes in the cloud top pattern around the eye can be detected using the Dvorak Enhanced IR approach, which employs a unique enhancement known as the IR-BD curve. It lists the four most common TC pattern kinds, including Eye pattern, curved band pattern, Shear pattern, and Central dense overcast (CDO) pattern.

The temperature difference between the warmest area of the eye and the coldest surrounding convection within 55 km is identified by the eye pattern (e.g., Fig. 10). The system is more robust the bigger the temperature contrast.

The concept behind the curved band pattern is that the system vorticity increases with the amount of wrapping around the rain bands. In comparison to IR photos, the curved band pattern is frequently simpler to see in visible photographs.

The CDO is the region that is surrounded by cirrus clouds that originate from thunderstorms in a TC's eyewall and rain bands. A stronger system is indicated by a low-level center that is more involved in the deep convection, according to the shear pattern, which looks at the distance between the low-level center and the CDO. The size and level of banding are used to evaluate the CDO's appearance.

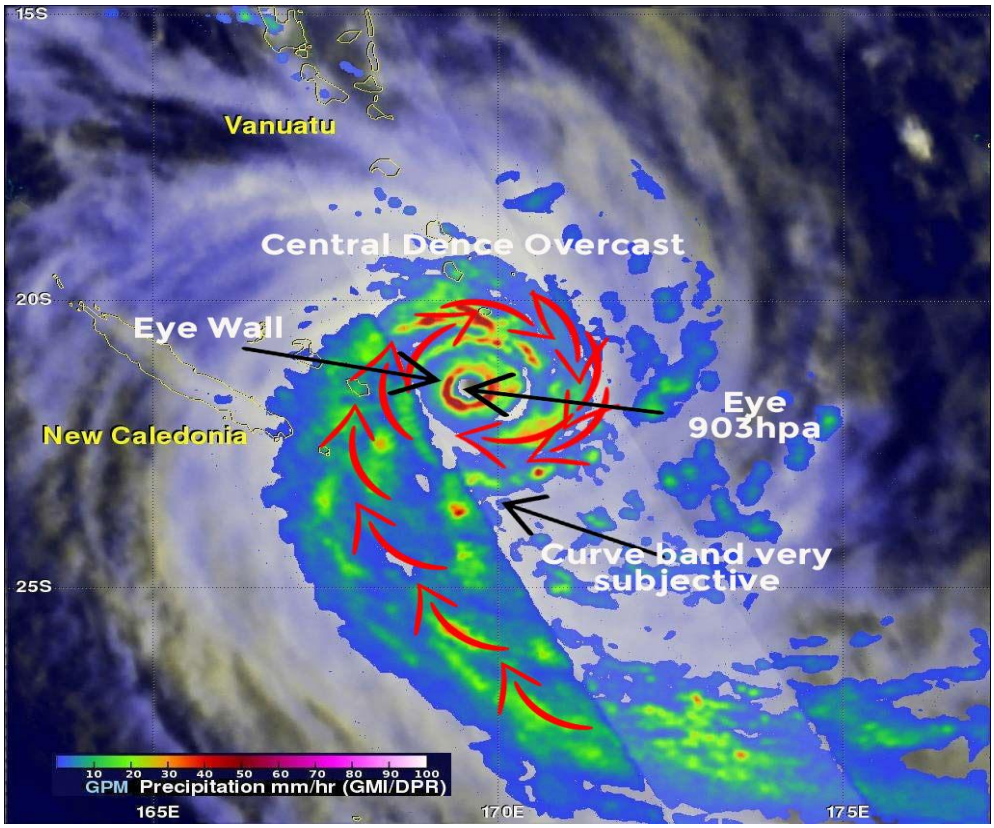

Figure 10. Sample identification of the Dvorak eyewall pattern, curved band pattern, and CDO.

Current intensity (CI)	MSW (kts)	MSLP (hPa)
		West Pacific
1.0	25	
1.5	25	
2.0	30	1000
2.5	35	997
3.0	45	991
3.5	55	984
4.0	65	976
4.5	77	966
5.0	90	954
5.5	102	941
6.0	115	927
6.5	127	914
7.0	140	898
7.5	155	879
8.0	170	858

Table 1. Summary of the Dvorak Western Pacific Wind-Pressure Relationship.

Digital IR data and objective algorithms based on the original empirical connections have been used to update and automate the Dvorak Technique.

Prior to the Advanced Objective Dvorak Technique (AODT) and as of 2006, the Advanced Dvorak Technique, there was the Objective Dvorak Technique (ODT) (ADT).

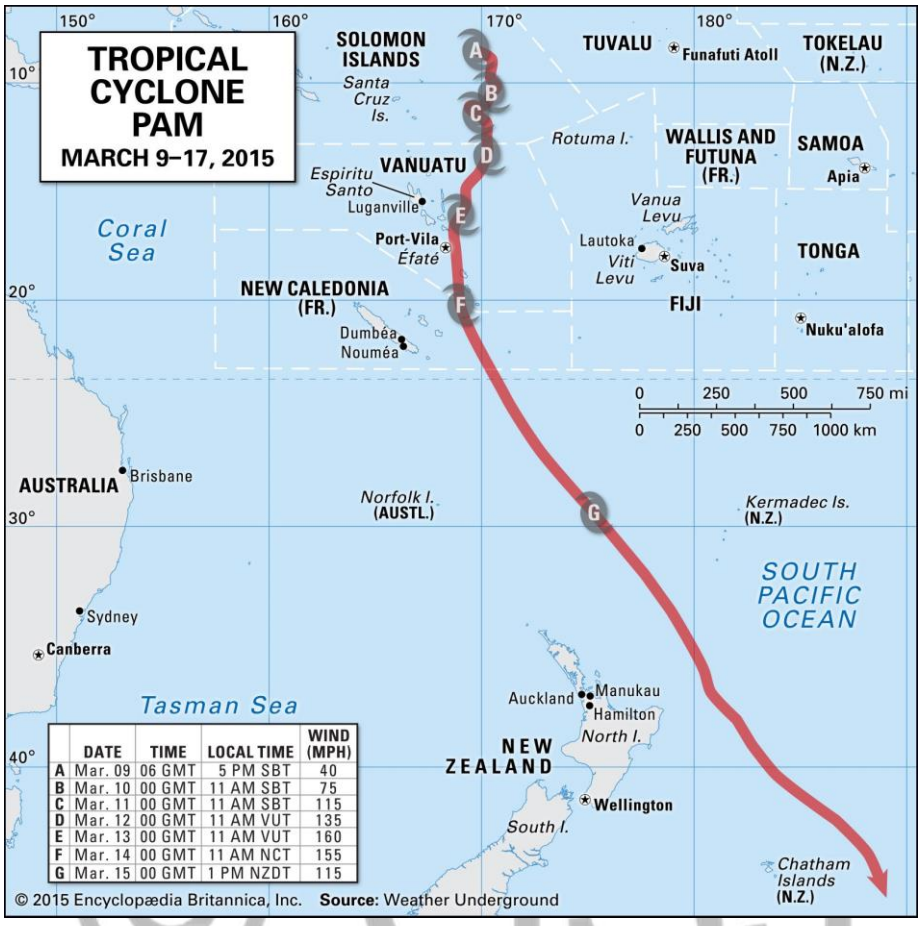

	DATE	TIME	LOCAL TIME	WIND (MPH)
A	Mar. 09	06 GMT	5 PM SBT	40
B	Mar. 10	00 GMT	11 AM SBT	75
C	Mar. 11	00 GMT	11 AM SBT	115
D	Mar. 12	00 GMT	11 AM VUT	135
E	Mar. 13	00 GMT	11 AM VUT	160
F	Mar. 14	00 GMT	11 AM NCT	155
G	Mar. 15	00 GMT	1 PM NZDT	115

Figure 11. TC Pam Wind (MPH) estimation by Britannica.Inc

When severe TC intensify or weaken, the concentric eyewall phenomenon or eyewall replacement cycle is frequently seen (those with winds greater than 50 m s-1, 115 mph). TC eyewalls often constrict as they get severe enough to cross the TC threshold. The TC starts a weakening phase once the existing eyewall has shrunk to its smallest size for that threshold intensity. The TC weakens as an outer eyewall arises because some of the moisture and momentum are taken from the original eyewall, which evaporates, all other things being equal. The TC eventually regains or acquires strength as the outer eyewall gradually contracts.

As massive TC Pam moved south of Vanuatu, it decreased in strength from category 5 to category 4, in part due to an eyewall replacement cycle, the satellite image is show in figure 12.

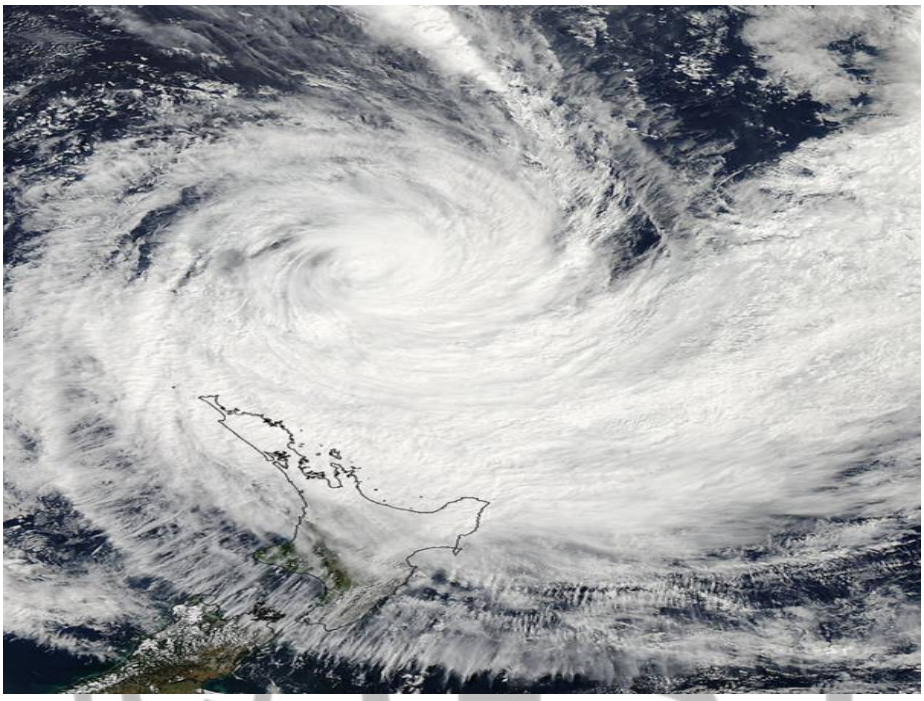

Figure 12. Satellite image of TC Pam eyewall replacement

The time between eyewall replacement cycles ranges from 12 to 18 hours or two to three days (e.g., Fig. 12). One or more eyewall replacement cycles are performed by some intense of TC Pam because TC Pam travels further over the ocean before running over New Zealand and with cool SST with other unfavorable environmental factors contributes to the highest percentage of strong storms with double eyewall structures.

Coastal flooding is where climate change has the most immediate impact on how TC affects the population. TC Pam typically causes two types of damage: (i) abnormally strong winds that directly harm constructed infrastructure and the environment, and (ii) widespread coastal flooding brought on by the storm surge that a TC Pam generates and the heavy rain that frequently precedes the storm.

Due to the global rise in sea levels brought on by the warming of the oceans and the melting of the ice sheets, storm surges are now riding on higher levels than they did previously, increasing the risk of flooding. The extent and severity of flooding damage from TC and other weather systems that can drive storm surges. Since the middle of the 19th century, the global sea level has already increased by around 20 cm and continues to rise, with an extra estimated rise from 40 centimeters to over a meter by 2100 compared to 1990s levels.

The increasing temperature of the surface of the ocean affects the intensity of TC because the storms draw energy from the surface waters of the ocean. This might speed up the wind and cause more rain. The sea surface temperature in TC Pam trajectory was well above average (Figure 13).

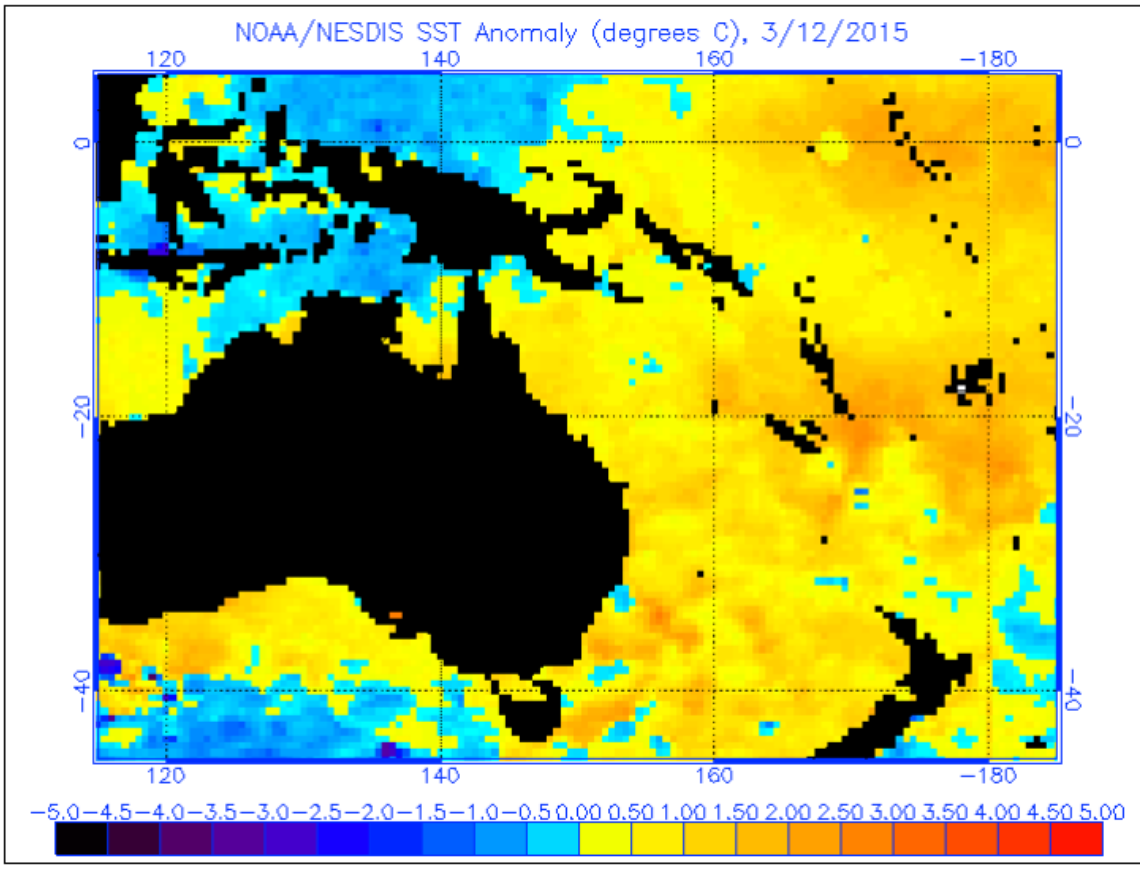

Figure 13. Sea surface temperature anomaly over the western pacific region, 12 march 2015.

TC is expected to become more powerful but less common overall. However, the impact of climate change thus far on the characteristics of TC is less well understood, in part because of the small and inconsistent datasets on TC behavior during the previous few decades.

Since the late 1970s, IPCC issued a warning regarding the upward trends in the north Atlantic, and weaker upward trends in the western north Pacific have been observed in time series of TC indices, such as power dissipation, an aggregate compound of TC duration, frequency, and intensity that measures total wind energy by TC

(IPCC, 20135). However, data quality concerns once again limit the interpretation of longer-term trends.

5. Summary and Concluding remarks.

Both major and minor disasters can be captured and recovered by using remote sensing. “Tracking the development and evolution of cloud systems, determining the TC intensity, researching its path and behavior, identifying and tracking the TC origination, and providing an early warning that ...” Remote sensing and numerical models can be crucial to hypothesize and estimate the maximum possible intensity of an event and its turbulence intensity and to make simulations of its evolution, providing important input for civil protection in the southwest pacific.

TC Pam in 2015 provided interdisciplinary scholars from several domains with the opportunity to investigate and test methods enabled by remote sensing. The largest storm surge in the Pacific region was created by TC Pam. On March 13, 2015, TC Pam made landfall in Vanuatu Islands. It had sustained gusts of up to 165 mph, extraordinary storm surges of more than 30 feet, and TC-force winds that extended 165 miles from its center. More than 11 people were murdered with many other injuries and Thousands of homes, schools, and buildings were damaged or destroyed, with an estimated 65,000 people displaced as a result. The lowland area and Coastal area were flooded, and public and commercial buildings, highways, bridges, water and electricity distribution systems, wastewater treatment facilities, and vital communication networks were all damaged by TC

Pam. Damage to hospitals and communication networks rendered affected towns helpless. The Vanuatu meteorology source states that it began as a tropical depression in the east of the Solomon Islands on March 6, 2015, strengthened to a TC Pam, and proceeded to make landfall on the islands of Vanuatu. Within the Vanuatu region, Pam quickly intensifies into a category 5 cyclone with 13.4m (44 feet) waves and maximum sustained winds of 280 km/h (175 mph).

The Capital of Vanuatu and other Area situated below sea level were breached by TC Pam's powerful winds and strong storm surges, according to the literature, flooding roughly 90% of the city which cause great significant economic and environmental damage.

According to a contributor, Pam was one of the most destructive and expensive cyclones to strike Vanuatu with estimated damages in excess of $450 million, and enacted two additional appropriation bills totaling $ 692 million for emergency response and recovery needs. Tourism, port operations (transportation and warehousing), arts, entertainment, recreation, lodging, and educational services all had a significant impact.

In order to identify TC damage in 2015, the users of satellites (low, moderate, and high-resolution) and aerial photographs. Rapidly gathered and made available remote sensing data from satellite and aerial platforms allowed for post-Pam situation assessment and reaction in Vanuatu. While meteorological satellites tracked the TC path, floods and surge inundation prevented terrestrial access, making remote sensing photography one of the first places to look for damaged data. According to the low-resolution satellite imagery and post-TC flood levels on March 15, 2015, one day after TC made landfall within Vanuatu Island. From the northern to the southern

island of Vanuatu, statistical comparing analyses were carried out a few days before moderate-resolution satellite photos on March 15, 2015, showing flooding extent in Low land Area. Photos were analyzed a few months later to follow the development of rising and receding flood levels on all the islands of Vanuatu.

High-resolution satellite imagery highlighted building details and gave a clear and comprehensive picture of the damage that had been seen. The integration of (high-resolution) satellite imagery and aerial images clearly demonstrates its importance and utility in assessing damage to buildings, roads, and other infrastructures, identifying the most stricken and needy areas, estimating the socio-economic effects of the disaster, and better predisposing and organizing. This context of data collection and dynamic archiving promotes reconnaissance and emergency planning.

TC Pam was a particularly potent storm that is thought to have cost the most money and been one of the first deadliest to ever hit the southwest Pacific Region, especially Vanuatu.

The development of TC Pam required the interaction of tropical storm Betty which originated in the Philippian and the trade winds move to the Pacific Ocean responsible for the strongest trade wind reversals ever observed, much like the formation of numerous TC in the Pacific basin. The atmospheric wave developed into Tropical Depression and quickly gained strength on a southward path over the Solomon Islands after colliding with weather remnants of a previous tropical depression north of Australia and the progressive weakening of an upper tropospheric mid-latitude deep trough (a significant intrusion of relatively colder air and its corresponding vertical wind

shear) (Figure 14). Both of these conditions are favorable for the development of a tropical cyclone.

Based on observation of the wind data the TC became Pam, which was the 11th tropical storm of the 2015 South-west tropical season, at about 12.00 UTC on 6 March, centered within the region of Fiji around 1,140 km to the north-west of Nadi, Fiji. The storm began southwest (Figure 15a). On March 9, a strong medium to the upper tropospheric high-pressure ridge over the Pacific Ocean and north of Vanuatu, caused it to develop an inner core and become a deeper TC. This ridge turned TC Pam southwest toward Vanuatu on March 11. TC Pam produced a powerful deep convection burst above the low-level core in the afternoon of 12 March 2015 over northern Vanuatu. TC Pam became a TC category 5 at 21.00 UTC on 12 March, four hours before hitting Vanuatu (Figure 14).

At 1500 UTC on 12 March, the highest sustained winds increased by up to about 135 knots (155.4 mph) making it a strong Category 4 TC on the Saffir-Simpson Wind Scale. Early on 12 March, an eye was seen in infrared satellite imagery, and by noon, the storm had a diameter of more than 340 nautical miles (629.7 km), with TC-force winds extending outward 30 nautical miles (55.5 km) and tropical-storm-force winds reaching as far as 170 nautical miles (314.8 km).

By March 12, its center was located around 521 nautical miles (965 kilometers) north-northeast of Noumea (New Caledonia), at latitude 14.7 south and longitude 169.8 east. TC Pam was traveling at 8 knots (14.8 kph) in a south-southeasterly direction.

After delivering tropical storm-force winds and significant rainfall across the southwest pacific on March 12, Pam continues moving

south toward Vanuatu (Figure 14) due to favorable deterioration in the large-scale air circulation that had kept TC Pam on a southeast-southward course.

The new eyewall had narrowed into a ring at 00.00 UTC on March 13 and a second, faster intensification had started. In less than 12 hours, Pam strengthened to a Category 5 Cyclone, reaching 150 knots (277.8 kph) around 0400 UTC on March 13. On March 13, Pam reached its maximum speed of 250 km/h, over Vanuatu. A GOES-12 satellite image of cyclone pam in the visible spectral band is shown in Figure 15b. That afternoon, the cyclone pressure dropped to a minimum of 896 bar. Figure 12 depicts TC Pam size in the northeast of New Zealand.

The connection with the ground was too brief for TC Pam to suffer a significant weakening.

The convective pattern of TC Pam was somewhat asymmetrical as it moved across Vanuatu, with the greatest winds and most intense rainfall occurring over Vanuatu Island (red area in Figure 15b). With maximum sustained winds of 160 mph, TC Pam quickly regained the status of a TC category 5 on 13 march with 155 mph (250 kph) winds. Located beneath a very massive upper-level anticyclone that, by March 13, had moved south of Vanuatu toward New Zealand. TC Pam began to rapid intensification on March 14 to march 20, these periods show TC Pam undergo relatively weak wind shear and efficient upper-level outflow.

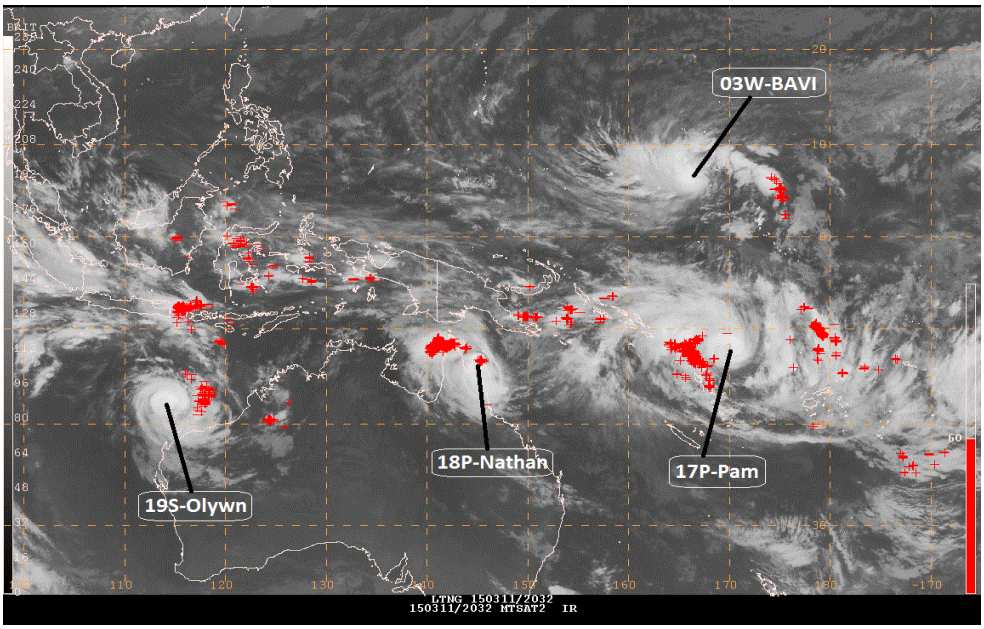

Figure 14. TC in the southwest pacific on march 13th 2015.

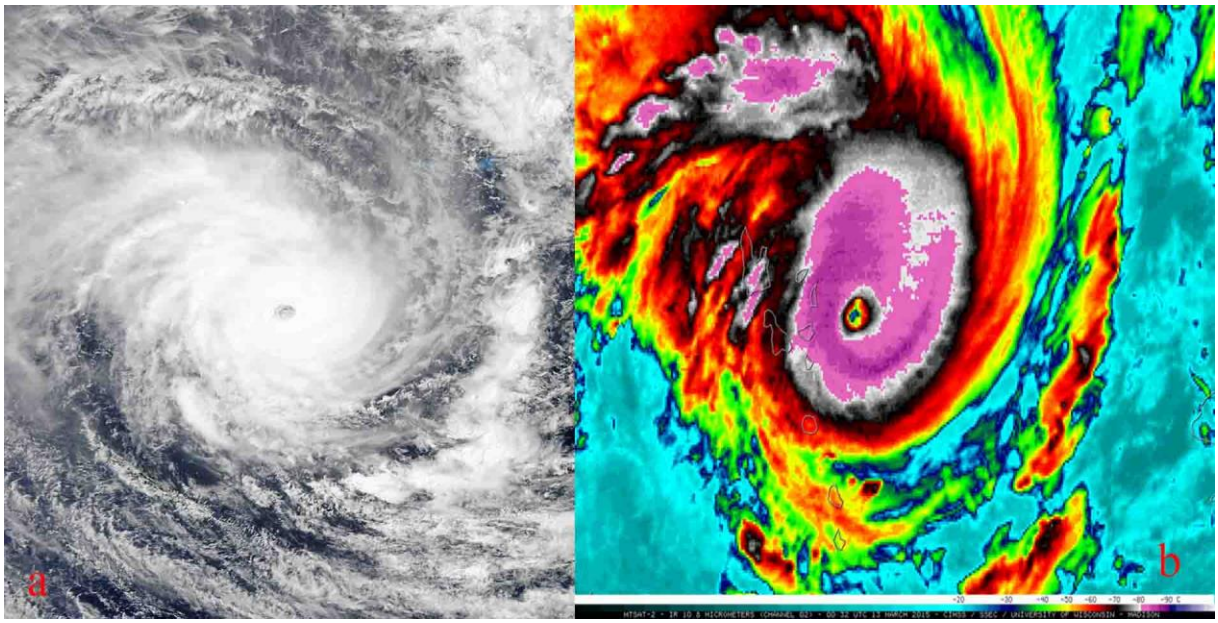

Figure 15. Satellite and radar image of TC Pam, (a). The movement of TC Pam towards Vanuatu; (b) TC Pam within the island of Vanuatu, on March 13th, 2015.

TC Pam remained a powerful category 4 TC despite the entrainment of dryer air and an opening of the eyewall to the south and northeast

of New Zealand on the morning of 14th march, despite the fact that TC of category 5 strength is rarely sustained for any length of time (due to internal dynamics).

Figure 6, 7, 9, and 11 illustrates how data collected via remote sensing techniques greatly aid in monitoring cyclones. Using several spectral bands and benefiting from their distinctive spectral fingerprints. Similar to a real eye, the super-spectral MERIS device tracks TC Pam in visible spectral bands, exposing swirling cloud patterns around the central eye and making the eyewalls visible. The Synthetic Aperture Radar (ASAR) on the ESA Envisat satellite captured an image of the cyclone on the left in the microwave C-band region of the electromagnetic spectrum, or through e.m. pulses with a wavelength of 10 cm: this suggests that the information provided by the radar energy backscattered to the ASAR by the target "illuminated" by the radar pulses includes information on the object's size, surface roughness, and electric properties. In this ASAR image, the 40x30 km2 central dark area represents a smoother sea surface because there are no winds at the extreme low-pressure center. This area is surrounded by a whitish sea surface that is very rough and has high radar backscatter, which includes a dark ring that was likely created by the very strong radar energy attenuation brought on by large thunderstorms with heavy rainfall.

TC in the southwest pacific was observed and analyzed by different satellite and radar remote sensing, the GEO IR/VIS is highly helpful in tracking TC development; however, it cannot provide precise estimates of the positions and intensities of TC centers. Because they can measure air profiles, LEO PMW sensors are better adapted for spotting TC genesis, development, and structures.

The PMW readings can be used to infer the TC structure and intensity.

An essential factor of TC operations is heavy precipitation. The availability of TC precipitation is essential for the places affected by drought since even a single TC precipitation process could significantly alleviate the dire drought situation. However, one of TC's effects for loss of life and property losses is the heavy rains brought on by its activity.

The asymmetric nature of TC rainfall makes TC rainfall distribution difficult to anticipate.

A more consistent TC rainfall from different PMW sensors and the TC diurnal characteristics are required to make further improvements in TC rainfall forecasts, even though accurate rainfall retrievals from PMV sensors and contemporary TC rainfall prediction schemes have led to reasonable TC rain forecasts.

When using data assimilation to improve TC forecasts, satellite remote sensing is crucial. The NWP model's beginning circumstances are improved, and the innovation error is minimized to produce better forecasts, using near real-time measurements of precise atmospheric conditions from LEO and GEO sensors. The capacity of the LEO PMW sounding sensors to produce precise air temperature and humidity profiles makes them particularly important for improving weather forecasts. With the development of better NWP models and data assimilation techniques over the past few decades, the forecast errors for the TC track have been gradually and significantly reduced.

Despite being statistically significant, the reduction of TC intensity prediction errors has a substantially lower improvement than the

reduction of TC track forecast errors. In addition to advancements in the next-generation NWP models and developments, future advanced satellite sensors on adequate satellites are required for better spatial and temporal global coverage. These efforts must focus on the best combinations of the combined satellite sensor channels that have positive impacts and better data assimilation methods.

Only data fusion from many satellite sensors can provide a comprehensive picture of TC operations worldwide. The LEO PMW sensors are advantageous for TC structures because of their great spatial resolution while polar-orbital satellites could only offer measurements, they lack temporal data but had correct TC placements, intensity analysis, and precipitation distributions twice a day over one place and frequent TC activity observation with LEO IR/VIS sensors has advantages, they fall short in terms of accurate TC eye positions, intensity analysis, and horizontal architecture ARCHER is a sophisticated algorithm that can accurately fix the TC center positions from PMW and IR/VIS sensors in close to real-time. The track of ARCHER offers top-notch TC positions for initialization in model TC data assimilation procedures and monitoring of TC activity. Evolutions of the TC live track from PMW sensors will be showing TC shapes and intensity for better forecasting and monitoring.

Acknowledgment

The author wishes to express sincere thanks to National Oceanic and Atmospheric Administration (NOAA), for making Satellite and Radar image data available.

Declarations

Conflict of interest the author has no conflicts of interest to declare that are relevant to the content of this article.

Reference

[1] Gray, W.M.: The formation of tropical cyclones. Meteorol. Atmos. Phys., 1998; 67, 37– 69

[2] TIROS – NASA Science: Accessed on April 28, 2016, http://science.nasa.gov/missions/ tiros/

[3] World bank, Cyclone Pam,NO.1, world bank,https://www.gfdrr.org/sites/default/files/publication/infographic-cyclone-pam.pdf

[4] Vanuatu, Post-disaster needs assessment executive summary,PRP VAN 49319,cyclone pam road construction project,https://www.adb.org/sites/default/files/linked-documents/49319-001-sd-01.pdf

[5] Vanuatu meteorology & Geo-hazard department: Accessed on november 01,2022, https://www.vmgd.gov.vu/vmgd/index.php/forecast-division/tropical-cyclone#:

[6] NOAA, Tropical cyclone climatology, NWS, https://www.nhc.noaa.gov/climo/?text#:

[7] Met office,Tropical cyclone facts,met office college, https://www.metoffice.gov.uk/research/weather/tropical-cyclones/facts#

[8] Sky Brary, low level wind shear,weather,https://www.skybrary.aero/articles/low-level-wind-shear

[9] Velden, C., and coauthors: The Dvorak tropical cyclone intensity estimation technique: a satellite-based method that has endured for over 30 years. Bull. Amer. Meteor. Soc., 2006; 87, 1195–1210.

[10] Dvorak, V.F.: Tropical cyclone intensity analysis using satellite data. NOAA Technical Report NESDIS 1984; 11, 1–47.

[11] Knapp, K.R., Kruk, M.C., Levinson, D.H., Diamond, H.J., and Neumann, C.J.: The International Best Track Archive for Climate Stewardship (IBTrACS). Bull. Amer. Meteor. Soc., 2010; 91, 363–376

[12] Olander, T.L. and Velden, C.S.: The advanced Dvorak technique: continued development of an objective scheme to estimate tropical cyclone intensity using geostationary infrared satellite imagery. Wea. Forecasting, 2007; 22, 287–298.

[13] Velden, C.S., Olander, T.L., and Zehr, R.M.: Development of an objective scheme to estimate tropical cyclone intensity from digital geostationary satellite infrared imagery. Wea. Forecasting, 1998; 13, 172–186.

[14] Kossin, J.P., Knaff, J.A., Berger, H.I., Herndon, D.C., Cram, T.A., Velden, C.S., Murnane, R.J., and Hawkins, J.D.: Estimating hurricane wind structure in the absence of aircraft reconnaissance. Wea. Forecasting, 2007; 22, 89–101.

[15] Knaff, J.A., Longmore, S.P., and Molenar, D.A.: An objective satellite-based tropical cyclone size climatology. J. Climate, 2014; 27, 455–476.

[16] Ritchie, E.A., Valliere-Kelley, G., Piñeros, M.F., and Tyo, J.S. Tropical cyclone intensity estimation in the North Atlantic basin using an improved deviation angle variance technique. Wea. Forecasting, 2012; 27, 1264–1277.

[17] Olander, T.L. and Velden, C.S.: Tropical cyclone convection and intensity analysis using differenced infrared and water vapor imagery. Wea. Forecasting, 2009; 24, 1558–1572.

[18] Chao, C.-C., Liu, G.-R., and Liu, C.-C.: Estimation of the upper-layer rotation and maximum wind speed of tropical cyclones via satellite imagery. J. Appl. Meteor. Climatol., 2011; 50, 750–766.

[19] Rappaport, E.N., and Coauthors: Advances and challenges at the national hurricanecenter. Wea. Forecasting, 2009; 24, 395–419.

[20] Chavas, D.R. and Emanuel, K.A.: A QuickSCAT climatology of tropical cyclone size. Geophys. Res. Lett., 2010; 37, L18816, doi:10.1029/2010GL044558.

[21] Chan, K.T.F. and Chan, J.C.L.: The size and strength of tropical cyclones inferred from QuikSCAT data. Mon. Weather Rev., 2012; 140, 811–824.

[22] Kimball, S.K. and Mulekar, M.S.: A 15-year climatology of North Atlantic tropicalcyclones. Part I: size parameters. J. Climate, 2004; 17, 3555–3575.

[23] Weatherford, C.L. and Gray, W.M.: Typhoon structure as revealed by aircraft recon-naissance. Part I: data analysis and climatology. Mon. Weather Rev., 1988, 116, 1032–1043

[24] Jiang, H., Ramirez, E.M., and Cecil, D.J.: Convective and rainfall properties of tropical cyclone inner cores and rainbands from 11 years of TRMM data. Mon. Weather Rev., 2013; 141, 431–450.

[25] Li, X., Zhang, J.A., Yang, X., Pichel, W.G., DeMaria, M., Long, D., and Li, Z.: Tropicalcyclone morphology from spaceborne synthetic aperture radar. Bull. Amer. Meteor.Soc., 2013; 94, 215–230.

[26] Hawkins, J.D., Lee, T.F., Turk, J., Sampson, C., Kent, J., and Richardson, K.: Real-timeinternet distribution of satellite products for tropical cyclone reconnaissance. Bull.Amer. Meteor. Soc., 2001; 82, 567–578.

[27] Kidder, S.Q., Gray, W.M., and Vonder Haar, T.H.: Estimating tropical cyclone central pressure and outer winds from satellite microwave data. Mon. Weather Rev., 1978; 106,1458–1464.

[28] Brueske, K.F. and Velden, C.S.: Satellite-based tropical cyclone intensity estimation using the NOAA-KLM series Advanced Microwave Sounding Unit (AMSU). Mon. Weather Rev., 2003; 131, 687–697.

[29] Kidder, S.Q., Goldberg, M.D., Zehr, R.M., DeMaria, M., Purdom, J.F., Velden, C.S.,Grody, N.C., and Kusselson, S.J.: Satellite analysis of tropical cyclones using the Advanced Microwave

Sounding Unit (AMSU). Bull. Amer. Meteor. Soc., 2000; 81, 1241–1259.

[30] Demuth, J.L., DeMaria, M., and Knaff, J.A.: Improvement of advanced microwave sounding unit tropical cyclone intensity and size estimation algorithms. J. Appl. Meteor. Climatol., 2006; 45, 1573–1581.

[31] Hawkins, J. and Velden, C.: Supporting meteorological field experiment missions and post-mission analysis with satellite digital data and products. Bull. Amer. Meteor. Soc., 2011; 92, 1009–1022.

[32] Herndon, D. and Velden, C.: Estimating tropical cyclone intensity using the SSMIS and ATMS sounders. Ext. Abst. 30th AMS Hurr. Conf., Ponte Verde Beach, FL., P1.21, 5p, 2012. [Available online at https://ams.confex.com/ams/30Hurricane/webprogram/Paper205422.html]

[33] Wimmers, A.J., and Velden, C.S.: MIMIC: a new approach to visualizing satellite microwave imagery of tropical cyclones. Bull. Amer. Meteor. Soc., 2007; 88, 1187–1196.

[34] Bankert, R.L., and Tag, P.M.: An automated method to estimate tropical cyclone intensity using SSM/I imagery. J. Appl. Meteor., 2002; 41, 461–472.

[35] Jones, T.A., Cecil, D., and DeMaria, M.: Passive-microwave-enhanced statisticalhurricane intensity prediction scheme. Wea. Forecasting, 2006; 21, 613–635.

[36] Olander, T.L., and Velden, C.S.: Current status of the UW-CIMSS Advanced Dvorak Technique (ADT). Preprints, 30th Conference on Hurricanes and Tropical Meteorology, Ponte Vedra

Beach, FL, Amer. Meteor. Soc., 2012; 7C.1/P1.19. [Available online at:https://ams.confex.com/ams/30Hurricane/webprogram/Paper204529.html]

[37] Kieper M.E. and Jiang, H.: Predicting tropical cyclone rapid intensification using the37 GHz ring pattern identified from passive microwave measurements. Geophys. Res.Lett., 2012; 39, L13804

[38] Gray, W.M.: Hurricanes: their formation, structure, and likely role in the tropical circulation. In: Meteorology over the Tropical Oceans, D.B. Shaw, Ed., Roy. Meteor. Soc.,1979; 155–218 pp. James Glaisher House, Grenville Place, Bracknell, Berkshire, RG121BX.

[39] Sadler, J.C.: The first hurricane track determined by meteorological satellite. Preprints from the 2nd Technical Conference on Hurricanes, Miami Beach, FL, Amer. Meteor. Soc., 1961. 13 pp.

[40] GOES history: Accessed on April 28, 2016, http://www.goes-r.gov/mission/history.html

[41] Antalovich J., "Disaster Response Aerial Remote Sensing Following Storms Irene and Lee", Photogrammetric Engineering and Remote Sensing, 77, 12, 2011, pp. 1185-1187.

[42] Joyce KE, Wright KC, Samsonov SV, Ambrosia VG (2009b) Remote sensing and the disaster management cycle. INTECH Open Access Publisher, Rijeka, Croatia

[43] Khan MSA (2008) Disaster preparedness for sustainable development in Bangladesh. Disaster Prev Manag 17:662-671

[44] Chiroiu L, Andre G Damage assessment using high resolution satellite imagery: Application to 2001 Bhuj, India, earthquake. In: Proc. 7th National Conference on Earthquake Engineering, 2001.

[45] Yamazaki F, Matsuoka M (2007) Remote sensing technologies in post-disaster damage assessment. Journal of Earthquake and Tsunami 1:193-210

[46] Lu D, Mausel P, Brondizio E, Moran E (2004) Change detection techniques. Int J Remote Sens 25:2365-2401

[47] Vatsavai R, Tuttle M, Bhaduri B, Bright E, Cheriyadat A, Chandola V, Graesser J Rapid damage assessment using high-resolution remote sensing imagery: Tools and techniques. In: Geoscience and Remote Sensing Symposium (IGARSS), 2011 IEEE International, Vancouver, Canada, 24-29 July 2011. IEEE, pp 1445-1448

[48] Al-Khudhairy D, Caravaggi I, Giada S (2005) Structural damage assessments from Ikonos data using change detection, object-oriented segmentation, and classification techniques. Photogrammetric Engineering and Remote Sensing 71:825

[49] Barnes CF, Fritz H, Yoo J (2007) Hurricane disaster assessments with image-driven data mining in high-resolution satellite imagery. Geoscience and Remote Sensing, IEEE Transactions on 45:1631-1640

[50] Eklund PW, You J, Deer P Mining remote sensing image data: an integration of fuzzy set theory and image understanding techniques for environmental change detection. In: AeroSense 2000, 2000. International Society for Optics and Photonics, pp 265-272

[51] Dewan AM (2013c) Vulnerability and Risk Assessment. In: Floods in a Megacity. Springer, pp 139- 177

[52] Yin J, Yin Z, Xu S (2013) Composite risk assessment of typhoon-induced disaster for China's coastal area. Nat Hazards 69:1423-1434. doi:10.1007/s11069-013-0755-2